

VERITAS: Verifying the Performance of AI-native Transceiver Actions in Base-Stations

Nasim Soltani*, Michael Löhning†, and Kaushik Chowdhury*

*Electrical and Computer Engineering Department, University of Texas at Austin, Austin, TX, USA

†National Instruments - Test and Measurement Group of Emerson, Dresden, Germany
nasim.soltani@utexas.edu, michael.loehning@emerson.com, kaushik@utexas.edu

Abstract—Artificial Intelligence (AI)-native receivers prove significant performance improvement in high noise regimes and can potentially reduce communication overhead compared to the traditional receiver. However, their performance highly depends on the representativeness of the training dataset. A major issue is the uncertainty of whether the training dataset covers all test environments and waveform configurations, and thus, whether the trained model is robust in practical deployment conditions. To this end, we propose a joint measurement-recovery framework for AI-native transceivers post deployment, called VERITAS, that continuously looks for distribution shifts in the received signals and triggers finite re-training spurts. VERITAS monitors the wireless channel using 5G pilots fed to an auxiliary neural network that detects out-of-distribution channel profile, transmitter speed, and delay spread. As soon as such a change is detected, a traditional (reference) receiver is activated, which runs for a period of time in parallel to the AI-native receiver. Finally, VERITAS compares the bit probabilities of the AI-native and the reference receivers for the same received data inputs, and decides whether or not a retraining process needs to be initiated. Our evaluations reveal that VERITAS can detect changes in the channel profile, transmitter speed, and delay spread with 99%, 97%, and 69% accuracies, respectively, followed by timely initiation of retraining for 86%, 93.3%, and 94.8% of inputs in channel profile, transmitter speed, and delay spread test sets, respectively.

Index Terms—AI-native air interface, AI-native receiver, OOD detection, adaptive receiver, channel change, NN-based receiver, 5G receiver, DeepRx.

I. INTRODUCTION

Artificial Intelligence native Air Interface (AI-AI) offers a fully AI-based wireless interface for next-generation wireless, where AI is integrated in both the data and control paths [1], [2]. AI-AI provides a myriad of flexibilities and opportunities for the physical layer design and implementation, including but not limited to: merging data decoding and application in the physical layer, providing flexibility in the choice of waveform with respect to the radio hardware and environment constraints, obviating costly hardware implementation for each individual processing block by being fully AI-based, reduction in standardization need, and the possibility of physical and MAC layer fusion [1], [2]. Furthermore, as data decoding and interpretation happens through neural networks (NNs) that have learned to map received data to originally transmitted bits, AI-based receivers have previously shown to yield lower bit error rate (BER) under low SNR conditions, compared to receivers with traditional signal processing blocks [3], [4].

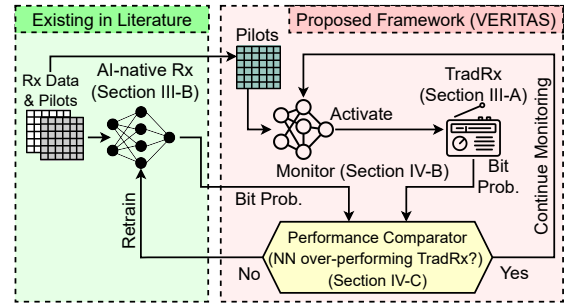


Fig. 1: VERITAS as the proposed framework for verifying the performance of AI-native Receivers. The Monitor continuously scans the wireless channel, and as soon as it detects a change, it activates a traditional receiver (TradRx). Then, bit probabilities of AI-native receiver and TradRx are compared to find the underperforming receiver. If necessary, a retraining process updates the AI-native receiver to adapt to the new environment.

Problem. Despite the several benefits that AI-AI provides for 6G communications, this newly proposed paradigm faces key challenges that need to be addressed before its successful deployment in 6G systems. For example, since wireless channel is a major contributor in the NN-based receiver performance, *verifying and maintaining the performance* of the AI-native receiver becomes a real challenge. NNs might not deliver the expected performance if they are deployed in an environment different from what they were trained in, as evident in several different examples: Recent work [5], [6] show that NN-based RF fingerprinting accuracy drops drastically when training channels are different from deployment channels. Authors in [3] show retraining is necessary to maintain the performance of an NN-based channel estimator in new environments. Authors in [7] show that automatic modulation classification performance drops when the environment changes, and propose transfer learning as an effective light retraining technique. The critical role of the wireless channel in AI/ML-based wireless systems renders the performance verification and maintenance of AI-AI necessary.

Preliminaries. As shown on the left side of Fig. 1, we assume an NN-based receiver (a.k.a., AI-native receiver) that is responsible for converting received wireless signals (Rx

Data & Pilots) to bits. Such models are well-explored in the literature in a number of prior works [8], [9], [10], [11], [12], [13], [3], [14]. Due to practical limitations, the training set of the NN-based receiver cannot contain all possible data variations or signals recorded under all possible channels encountered in the real world. Instead, the NN-based receiver is trained on a number of channel profiles, mobility conditions. While it performs well under the seen configurations, it is an open question whether it may suffer from a performance drop due to changes in the wireless environment (channel) during deployment.

Proposed Solution. On the right side of Fig. 1, we propose VERITAS – a framework for verifying the performance of AI-native receiver to ensure its maintained superior performance over the traditional receiver. VERITAS has 3 components: the Monitor, the traditional receiver (TradRx), and the Performance Comparator. The Monitor runs continuously in parallel to the AI-native receiver to observe the wireless channel and detect potential changes in the channel profile, transmitter speed, or delay spread. As soon as such a change is detected, TradRx is activated that is used as a comparison point against the AI-native receiver. The Performance Comparator compares output bit probabilities of the two receivers and determines which receiver is underperforming. Notably, this step does not require the true bit labels. If the AI-native receiver is identified as the underperforming receiver, a retraining process is initiated to lightly retrain the AI-native receiver. The proposed Performance Comparator in VERITAS is able to operate on encoded as well as raw (i.e., unencoded) bits, which obviates the need for a costly decoding block within the proposed framework.

Contributions. Our contributions are as follows:

- We propose VERITAS as a framework for verifying the performance of an AI-native receiver, to ensure its maintained superior decoding performance compared to traditional receiver (Section IV-A).
- To demonstrate VERITAS works for generic AI-native receivers, we choose a widely used NN-based 5G receiver called DeepRx [15] as our AI-native receiver (Section III-B), which is designed to give lower BER compared to the traditional receiver (TradRx). We extensively analyze DeepRx performance for different training and test set configurations, and determine configurations where DeepRx yields higher BER compared to TradRx (Section III-C).
- We propose an environment change detector called Monitor to identify any potential changes in one of the wireless channel properties of channel profile, transmitter speed, and delay spread. We design the Monitor as a NN-based out-of-distribution (OOD) detector, that extracts features out of received pilots, and uses a novel OOD detection algorithm based on K-nearest neighbor (KNN) for detecting environment changes (Section IV-B).
- We propose an analytical method based on histogram binning to compare the output bit probabilities of the AI-native receiver against those of TradRx as reference. The proposed Performance Comparator compares output bit probabilities at the deployment phase and without having

the true bit labels. This comparison determines if the AI-native receiver is underperforming with respect to the reference which initiates a retraining process (Section IV-C).

- We pledge to publicly release our code for VERITAS including pipelines for the Monitor and the Performance Comparator, upon the acceptance of this paper.

II. RELATED WORK

In this section, we summarize the closest related work in three different areas of AI-native receiver performance maintenance (Section II-A), wireless channel change detection (Section II-B), and OOD detection (Section II-C).

A. AI-native Receiver Performance Maintenance

The issue of performance drop in the NN-based receivers due to channel variations has been studied extensively. Authors in [16] propose a fixed time interval (periodic) retraining technique to adapt NN-based Orthogonal Frequency Division Multiplexing (OFDM) receivers to occasionally changing channel conditions. Naive periodic retraining is a way of maintaining performance of an NN-based receiver, however, it periodically imposes often unnecessary training computational complexity to the system as well as wastage of data frames that are used as the retraining dataset. Authors in [17] propose a denoising approach during training for learning OFDM channel coefficients. They construct their training set out of estimated channel coefficients of low noise signals, but dynamically add Additive White Gaussian Noise (AWGN) to inputs during training. This method makes the NN-based channel estimator robust to changes in the noise level, however, this does not solve the problem of transitioning between different wireless channels between training and deployment phases.

B. Wireless Channel Change Detection

Authors in [18] use the channel state information (CSI) of IEEE 802.11p signals for environment identification in V2V communication. They consider 5 different environments of rural line-of-sight (LOS), urban LOS, urban non-line-of-sight (NLOS), highway LOS, and highway NLOS for V2V communication and perform a multi-class classification using a deep convolutional NN, KNN, support vector machine, random forest, and Gaussian Naive Bayes algorithms. They show superior performance of the NN compared to the other algorithms, however, they do not go beyond the fixed training set environments and do not show any method for identifying new unseen environments. Authors in [19] classify speeds of users in a 5G network using the reference signal received power (RSRP) passed through a deep NN. They categorize speeds between 0 and ∞ km/h into 8 non-overlapping classes, with the last class spanning from 90 km/h to ∞ . This categorization encompasses all the possible speeds, however, simple speed classification without out-of-library detection does not satisfy the requirements in our proposed AI-AI maintenance framework.

C. Out-of-Distribution (OOD) Detection

Detecting OOD samples is a well-investigated problem in machine learning [20], [21]. In wireless communications, autoencoders have been vastly used for OOD detection. In such methods an autoencoder is trained to reconstruct an input, and the reconstruction error for known in-distribution (ID) inputs are averaged and recorded as a reference. At the deployment phase, all unknown inputs are fed to the autoencoder and their reconstruction errors are compared against the reference error. If the reconstruction error of the unknown test input is larger than the reference, the input is identified as an OOD input. Authors in [22] use a variational autoencoder and study the signal reconstruction error for identifying OOD modulation schemes. The disadvantage of autoencoder-based OOD detection is that completely different pipelines are needed for OOD detection and ID data classification. On the other hand, classification-based OOD detection methods provide a unified pipeline for both tasks. Authors in [23] detect unseen devices in the well-known RFMLS [24] WiFi and ADS-B datasets using a classification-based OOD detection method. They train their classifier NN with a custom loss function that has 3 components of intra-centroid loss, nearest neighbor loss and a final loss component that pushes the cluster centers away to spread in the space. However, their proposed method requires exposure of the NN to out-of-library devices (classes) that are not categorized into meaningful classes during training. Authors in [25] include a feature-based new device detection in their proposed LoRa RF fingerprinting scheme. They calculate the average of distances of each test feature from all of its K nearest neighbors. They compare this average distance to a predefined λ value, and decide if the device is OOD or has been seen during training. This feature-based OOD detection scheme, although light and efficient in real-time, has a few downsides. First, averaging the distances of the test feature from its K neighbors causes a lot of information regarding the individual distances from neighbors to be loss. Second, considering the distance of the test feature from its neighbors for OOD detection relies on the assumption that the ID points are close to each other and the OOD features are far from them. This limits the OOD detection scheme to work well only with ID clusters that are centrally dense and with only far OOD data.

In the rest of this paper, we introduce a widely used NN-based receiver as our example AI-native receiver, and explore its performance for different training and test set configurations. Then, we describe and evaluate VERITAS as a framework for verifying the performance of this AI-native receiver to avoid its naive periodical and often unnecessary retraining.

III. PRELIMINARIES

In this section, first we describe the data generation pipeline and the traditional receiver (TradRx) that are implemented in Python using *Sionna* libraries (Section III-A). Second, we describe the NN-based receiver that we use in this paper as our example AI-native receiver (Section III-B), and finally, we explore and study how the NN-based receiver performs

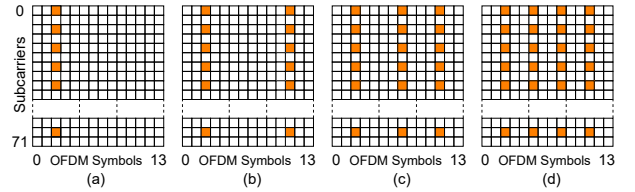


Fig. 2: Different 5G-NR pilot patterns for each OFDM subframe with 6 PRBs. Pilot OFDM symbol indices are set as (a) [2], (b) [2,11], (c) [2,7,11], and (d) [2,5,8,11].

compared to the TradRx in different training and test configurations (Section III-C). Specifically, we attempt to show cases where varying one of the parameters of channel profile, transmitter speed, and delay spread between the training and test sets increases the BER of the NN-based receiver above that of TradRx.

A. Data Generation and TradRx Pipeline: *Sionna*

Data Generation Pipeline. To generate 5G radio frames with different configurations for our training and test experiments, we implement a data generation pipeline using *Sionna* that is an open source Python library. *Sionna* enables the rapid prototyping of complex communication system architectures and provides native support for integration of NNs that are based on Tensorflow [26]. We implement a 5G transmitter that generates 5G radio frames with standard-compliant structure, grid size, and pilot patterns. To simulate the wireless channel, we use 3GPP 38.901 tap-delay line models of `tdl_a`, `tdl_b`, `tdl_c`, `tdl_d`, and `tdl_e`, that are implemented and available within *Sionna*. We also use the *Sionna* API `AWGN()` to add specific levels of noise to the data after wireless channel. Our data generation pipeline has the capabilities of simulating and generating large amounts of 5G data for a vast range of configurations, including but not limited to different pilot patterns, transmitter speeds, noise levels, delay spreads, and different channel models. The generated data is saved in different stages of the processing chain, such as at the transmit bit level, at the received frame level, etc., all in the signal metadata format (SigMF) [27].

Fig. 2 shows 4 different 5G-compliant pilot patterns. We select the number of physical resource blocks (PRBs) as 6 (i.e., 72 subcarriers) to reduce simulation time. However, the proposed method is generalizable to higher numbers of PRBs as well. Among different patterns in Fig. 2, without losing generality of the core method, we select pattern (c) for our implementations and experiments in the rest of this paper.

Traditional Receiver (TradRx) Pipeline. Apart from the design of transmitter, wireless channels and noise, we use *Sionna* APIs also to simulate a traditional 5G receiver that we refer to as TradRx. To implement TradRx, different *Sionna* classes and functions including `OFDMDemodulator`, `LSChannelEstimator`, `LMMSEEqualizer`, and `Demapper` are used. The implemented TradRx is used as a reference receiver for benchmarking the performance of the AI-native receiver for different datasets with different configurations.

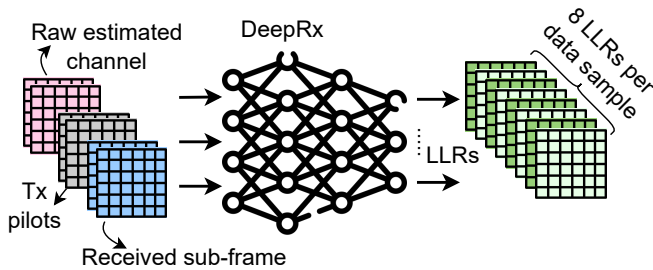


Fig. 3: Inputs and outputs of DeepRx model.

B. The 5G AI-native Receiver: DeepRx

As our AI-native receiver, we choose a widely used fully convolutional 5G receiver with 672k parameters called DeepRx [15]. DeepRx interprets frequency domain I/Q samples of 5G subframes to their corresponding softbits (a.k.a., log likelihood ratios (LLRs)) as outputs. The softbits represent output of the modulation symbol demapper in a traditional receiver, which are fed into the error correction block. As shown in Fig. 3, the inputs of DeepRx are 3 components: (i) the frequency domain received 5G subframe: that includes received data and pilots in the proper indices, where real and imaginary components are separated in the last dimension. The subframe has dimensions (14, 72, 2) that represent time, frequency, and real/imaginary parts, respectively. (ii) raw estimated channel coefficients: that occupy pilot indices in a matrix of zeros with size (14, 72, 2) where real and imaginary components come in the last dimension. (iii) transmitter-side pilot symbols: that occupy the pilot indices in a matrix of zeros with size (14, 72, 2) similar to the raw estimated channel matrix. These three matrices are concatenated in the last dimension to create an input with dimensions (14, 72, 6) for DeepRx. The output of DeepRx is a vector of 8 LLR values for each I/Q sample, that add up to $14 \times 72 \times 8 = 8064$ LLR values. This output size is designed to accommodate to the highest modulation scheme of 256QAM. However, a portion of the LLRs are invalid for lower modulation schemes and need to be filtered out for BER calculations. Specifically, the LLRs that fall in pilot indices and the most significant bits in LLRs that represent a higher modulation scheme than that of DeepRx input are invalid LLRs and must be filtered out. The DeepRx pipeline that we use in this paper is implemented in python using `Tensorflow-Keras` library. More details about DeepRx NN architecture can be found in [15]. We note that as the error correction block is not part of the DeepRx NN in [15], we also do not include this block in the implementation of either DeepRx or TradRx. Therefore, without losing generality of our proposed method, all the BER results reported in the rest of this paper are reported for *unencoded* bits.

C. Exploration of DeepRx Performance in Comparison to TradRx

One of the advantages of AI-native receivers is providing lower BER compared to the traditional receivers. Authors in [15], [28] show superior performance of DeepRx in terms of

BER compared to the traditional non-NN receiver, however, only limited training/test configurations are studied. Various cases where the training and test sets might differ in terms of channel profiles, speeds, etc., are not considered in [15]. In the real world, training the AI-native receiver on all possible wireless channels is not possible due to practical limitations. Therefore, the trained AI-native receiver might be deployed in completely new settings where any or all the wireless channel properties are different. In this case, DeepRx (or any general AI-native wireless receiver) might fail to outperform the traditional receiver.

In this subsection, we attempt to identify corner cases where DeepRx BER increases above the traditional receiver BER, and refer to them as “performance drop cases”. While we limit our studies to DeepRx as a widely used 5G receiver, our core method can be deployed to any general AI-native receiver.

Here, three different parameters of channel profile, transmitter speed, and delay spread are studied and the impact of their variations on the performance of DeepRx is explored. We perform 6 training experiments and provide detailed description for each experiment that renders them repeatable by interested readers. Key takeaways of these experiments are summarized at the end of Section III-C. For each experiment, the training and test datasets are created with the three parameters set to specific values, described with one or multiple configuration triples of (channel profile, transmitter speed, delay spread). Data modulation scheme is set to 16QAM for all the datasets, and additive white Gaussian noise in range $E_b/N_0 = 0$ to 20 dB with steps of 2 dB is generated and added to each 5G radio frame. Each training and test set contains 5000 and 500 uplink 5G radio frames, respectively, per E_b/N_0 level for each configuration triple. In each training run, the DeepRx model is fully trained for ~ 20 epochs. To measure TradRx BER and DeepRx BER in different E_b/N_0 levels, the corresponding test set is passed through the TradRx (described in Section III-A), and the trained DeepRx model (described in Section III-B), respectively, and BER versus E_b/N_0 is plotted in Figures 4-9. In all these figures, each marker represents a certain test configuration triple, and DeepRx and TradRx BER plots are shown using solid lines and dashed lines, respectively. It is expected that DeepRx BER is lower than TradRx BER in all E_b/N_0 (DeepRx outperforms TradRx), otherwise that specific training/test configuration is flagged as a *performance drop cases*.

1) Impact of Change in Channel Profile on DeepRx BER:

The wireless channel profile defines channel properties such as the number of reflections of the signal in the environment (a.k.a., number of channel taps), the relative delays between those reflections, and the signal attenuation caused by each reflection. To explore the impact of wireless channel profile types and find any potential *performance drop cases* we create two different training sets and perform two different experiments: Channel Profile - Exp. 1 and 2.

Channel Profile - Exp. 1: The goal of the first channel experiment is to investigate DeepRx performance when it is trained on a NLOS channel and tested on different channel profiles including NLOS and LOS. We create the first training set with configuration triple of (channel profile, transmitter

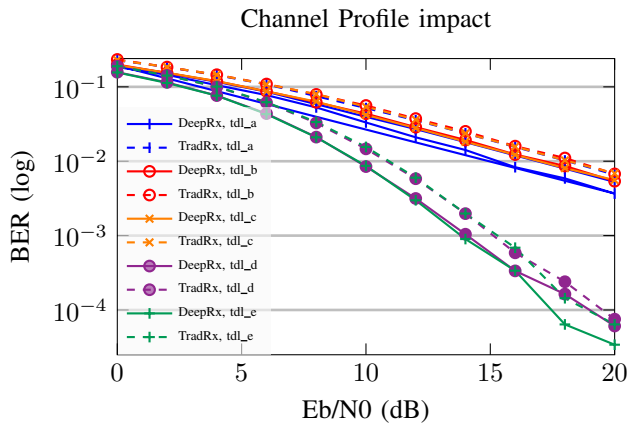


Fig. 4: BER vs. E_b/N_0 of Channel Profiles - Exp. 1, where DeepRx is trained on tdl_a (NLOS) channel. Test sets are passed through TradRx (dashed lines) and trained DeepRx (solid lines). It can be seen that all solid lines are below the dashed line with the same marker, DeepRx performs better than the TradRx in LOS and NLOS channel profiles, and therefore, no *performance drop case* is observed.

speed, delay spread) fixed as (tdl_a, 10 m/s, 400 ns). Here, tdl_a channel profile is selected as an example NLOS channel profile, and 10 m/s and 400 ns are chosen as arbitrary values for speed and delay spread parameters, respectively. After training DeepRx, we create five different test sets. In each test set we keep the speed and delay spread same as in the training set and set different channel profiles among the list of [tdl_a, tdl_b, tdl_c, tdl_d, tdl_e]. For each channel profile DeepRx BER and TradRx BER versus E_b/N_0 levels are shown in Fig. 4. As it can be seen for all of the test channel profiles, DeepRx outperforms TradRx by yielding lower BER, which shows the trained model is robust to channel profile changes between the training and deployment phases. This is due to the training set channel (NLOS) being equally or more complicated compared to the test channel profiles (NLOS/LOS), which leads to training a DeepRx model robust to channel profile changes.

Channel Profile - Exp. 2: To further explore the impact of change in the channel profile, we create a second training set with configuration triple of (channel profile, transmitter speed, delay spread) set as (tdl_d, 10 m/s, 400 ns). Here we choose tdl_d as an example LOS channel and keep speed and delay spread same as in Channel Profile - Exp. 1. After DeepRx model is trained, we test it on the five previously generated test sets with different channel profiles. Fig. 5 shows DeepRx and TradRx BER plots versus E_b/N_0 for the five test channel profiles. As it can be seen, DeepRx BER is below TradRx BER in all E_b/N_0 levels for tdl_d (LOS) (same channel as the training set) and tdl_e (LOS) (similar channel to the training set). However, BER of DeepRx increases above TradRx BER for some E_b/N_0 levels in test sets of NLOS channels (i.e., tdl_a, tdl_b, and tdl_c). This increase is up to 111% for tdl_a in $E_b/N_0=20$ dB. This shows that a *performance drop case happens if DeepRx is trained on LOS and tested on NLOS channel profiles*.

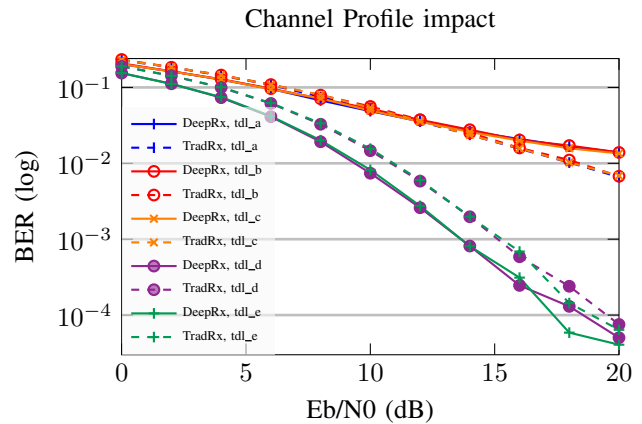


Fig. 5: BER vs. E_b/N_0 of Channel Profile - Exp. 2, where DeepRx is trained on tdl_d channel (LOS). Test sets are passed through TradRx (dashed lines) and trained DeepRx (solid lines). It can be seen that DeepRx performs worse than TradRx for tdl_a, tdl_b, and tdl_c (i.e., NLOS) test channels, and therefore, a *performance drop case* is observed.

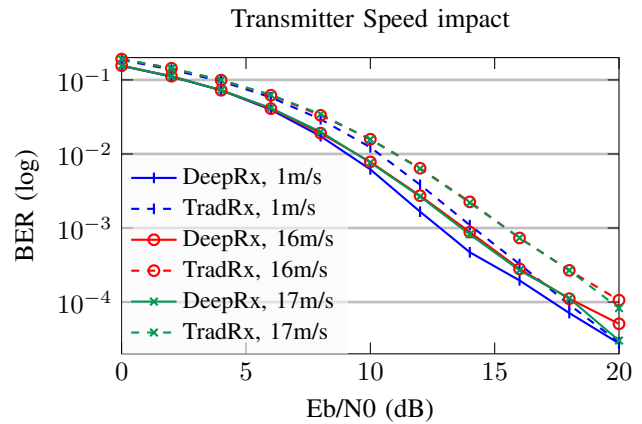


Fig. 6: BER vs. E_b/N_0 of Speed - Exp. 1 where DeepRx is trained on higher speeds of 18, 19, and 20 m/s. Test sets with lower speeds are passed through trained DeepRx (solid line) and TradRx (dashed line). For all test sets, the solid lines are below their corresponding dashed lines with the same marker, therefore, no *performance drop case* is observed.

2) Impact of Transmitter Speed Change on DeepRx BER:

Another parameter that can vary between NN-based receiver training and deployment phases is transmitter speed. An AI-native receiver could be trained on data collected with certain transmitter speeds, however, deployed in other speeds. To study the impact of change in speed on DeepRx performance, we design and run two experiments: Speed - Exp. 1 and 2.

Speed - Exp. 1: The goal of the first speed experiment is to see how DeepRx performs if trained on higher and deployed in lower speeds. We compose a training set with configuration triple of (channel profile, transmitter speed, delay spread) set as (tdl_d, 18 m/s, 400 ns), (tdl_d, 19 m/s, 400 ns), and (tdl_d, 20 m/s, 400 ns). In this case, we select transmitter speed to take different values of 18, 19, and 20 m/s, and channel profile and delay spread are arbitrarily selected as tdl_d and 400 ns.

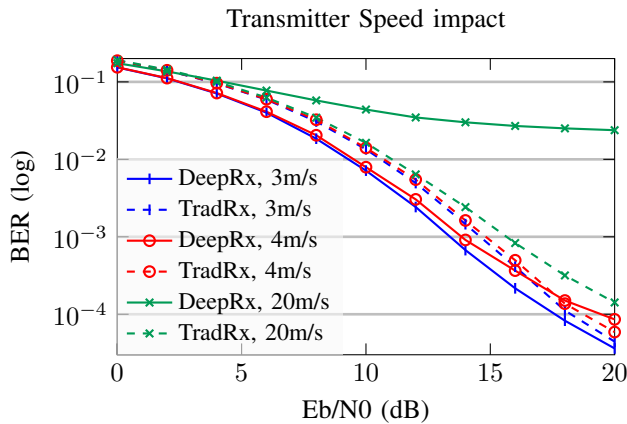


Fig. 7: BER vs. E_b/N_0 of Speed - Exp. 2 where DeepRx is trained on lower speeds of 0, 1, and 2 m/s. Test sets with higher speeds are passed through trained DeepRx (solid line) and TradRx (dashed line). In test speeds 4 m/s and larger, the solid line is above the dashed line which clearly shows a *performance drop case*.

After DeepRx is trained on this training set, we create three test sets to have the same channel profile and delay spread configurations as the training set but different speeds of 17, 16, and 1 m/s. The first two speeds of 17 and 16 m/s are chosen to be the next two lower speeds compared to the lowest speed in the training set (i.e., 18 m/s). The last speed of 1 m/s is selected as a lower speed that is far away from the training speed range. We plot BER versus E_b/N_0 results of DeepRx and TradRx in Fig. 6 and observe that in all test cases DeepRx BER is below TradRx BER, which means DeepRx outperforms TradRx if it is trained on higher and tested on lower speeds, therefore, *no performance drop cases* are observed.

Speed - Exp. 2: The purpose of the second speed experiment is to investigate DeepRx performance when trained on lower and tested on higher speeds. To do this, we create a training set with the same channel profile and delay spread as in Speed - Exp. 1 (i.e., t_{dl_d} and 400 ns) however, we chose the speeds to be 0, 1, and 2 m/s. Therefore, the training set comprises configuration triple of (channel profile, transmitter speed, delay spread) set as (t_{dl_d} , 0 m/s, 400 ns), (t_{dl_d} , 1 m/s, 400 ns), and (t_{dl_d} , 2 m/s, 400 ns). After training, we test DeepRx on three different test sets with the same channel profile and delay spread as the training set, but speeds of 3, 4, 20 m/s. In this case, 3 and 4 m/s are chosen to be the closest higher speeds with respect to the training speeds, and 20 m/s is chosen as a higher speed far away from the training speed range. We plot BER versus E_b/N_0 results of DeepRx and TradRx in Fig. 7 and observe that for 3 m/s test case that is 1 m/s higher than the training speed range, DeepRx BER is lower than TradRx BER. However, at 4 m/s that is 2 m/s higher than the training speed range, DeepRx BER starts to increase above TradRx BER. For 20 m/s test case which is a higher speed far away from the training speed range, DeepRx underperforms the TradRx with a larger gap of up to 16648% in $E_b/N_0 = 20$ dB. This shows that a *performance drop case might happen if DeepRx is tested on speeds that are 2 m/s or*

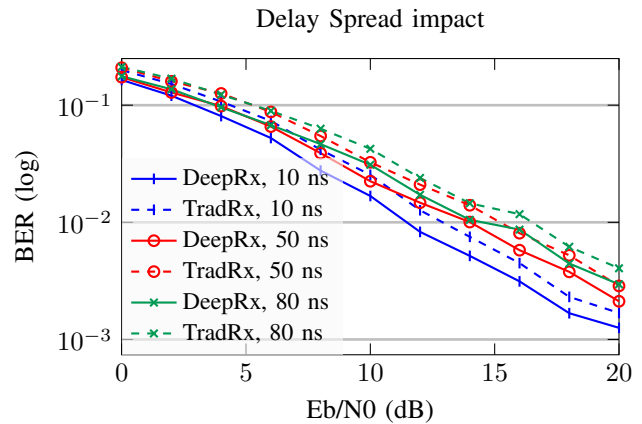


Fig. 8: BER vs. E_b/N_0 of Delay Spread - Exp. 1, where DeepRx is trained on high delay spreads of 400, 450, and 500 ns. Test sets with lower delay spreads are passed through trained DeepRx (solid lines) and TradRx (dashed lines). All solid lines are below their corresponding dashed lines with the same marker, therefore, *no performance drop case* is observed.

more higher than the training speed range.

3) *Impact of Change in Delay Spread on DeepRx BER:* The last parameter we study is the delay spread that is another important property of a wireless dataset. In a given environment, delay spread can change as the objects and obstacles in the environment change. Consequently an NN-based receiver can be trained in an environment with certain delay spread values, however, it can be deployed in another environment with other delay spread values. To study the impact of change in the delay spread between the training and test environments we design and implement two experiments: Delay Spread - Exp. 1 and 2.

Delay Spread - Exp. 1: The purpose of the first delay spread experiment is to investigate how DeepRx performs if it is trained on higher and deployed on lower delay spreads. We compose a training set with configuration triple of (channel profile, transmitter speed, delay spread) set as (t_{dl_b} , 2 m/s, 400 ns), (t_{dl_b} , 2 m/s, 450 ns), and (t_{dl_b} , 2 m/s, 500 ns). In this case, we select the channel profile to be a NLOS channel (i.e., t_{dl_b}) as the delay spread manifests a more significant impact in such channels. We select different delay spreads of 400, 450, and 500 ns as high delay spreads, and 2 m/s as a arbitrary value for speed. After DeepRx model is trained, we generate three test sets with the same channel profile and speed as the training set, however, we choose different delay spreads of 10, 50, and 80 ns as low delay spreads. We show BER results versus E_b/N_0 for DeepRx and TradRx in Fig. 8. We observe that for all test delay spreads DeepRx BER is below TradRx BER, which means DeepRx outperforms TradRx if it is trained on higher, and tested on lower delay spreads. In this case *no performance drop case* occurs.

Delay Spread - Exp. 2: The purpose of the second delay spread experiment is to investigate DeepRx performance when it is trained on lower and tested on higher delay spreads. To do this, we create another training set with configuration triple of (channel profile, transmitter speed, delay spread) set

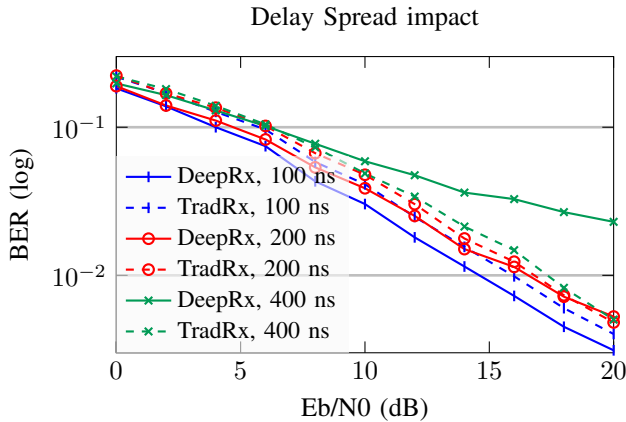


Fig. 9: BER vs. E_b/N_0 of Delay Spread - Exp. 2, where DeepRx is trained on lower delay spreads of 10, 50, and 80 ns. Test sets of higher delay spreads are passed through trained DeepRx (solid lines) and TradRx (dashed lines). For the 400 ns test set, the solid line is above the dashed line which clearly shows a *performance drop case*.

	Channel Profile Impact	Speed Impact	Delay Spread Impact
Training	Channel Profile	tdl_d	tdl_b
	Speed (m/s)	10	0, 1, 2
	Delay Spread (ns)	400	10, 50, 80
Test	Channel Profile	tdl_a, tdl_b, tdl_c	tdl_b
	Speed (m/s)	10	≥ 4
	Delay Spread (ns)	400	> 200 ns

TABLE I: Training and test configurations that led to DeepRx underperforming TradRx. It should be noted that the performance drop cases for DeepRx are not limited to these configurations, however, this table is identified as example configurations where DeepRx performance drop is observed.

as (tdl_b, 2 m/s, 10 ns), (tdl_b, 2 m/s, 50 ns), and (tdl_b, 2 m/s, 80 ns). In this case, we keep the channel profile and speed configurations same as Delay Spread - Exp. 1, but select different values of 10, 50, and 80 ns for delay spread. After DeepRx is fully trained, we create three different test sets with the same channel profile and speed as in the training set, but different delay spreads of 100, 200, 400 ns. We plot BER versus E_b/N_0 results of DeepRx and TradRx in Fig. 9 and observe that for delay spread of 100 ns, DeepRx BER is below TradRx BER. At 200 ns DeepRx starts to underperform the TradRx, even though only by a negligible margin in $E_b/N_0=20$ dB. In 400 ns DeepRx BER is above the TradRx BER with a larger gap of up to 357% in $E_b/N_0=20$ dB. This shows that a *performance drop case might happen if DeepRx is trained on lower and tested on higher delay spreads*.

• **Key take away:** We explored the performance of DeepRx with respect to TradRx in different training and test configurations. We showed that DeepRx might provide higher BER compared to TradRx in three different cases: (i) change in the channel profile: if DeepRx is trained on a LOS channel such as tdl_d and deployed in NLOS channel profiles such as tdl_a, tdl_b, and tdl_c. (ii) change in the transmitter speed: if DeepRx is trained on a specific speed range such as speeds 0, 1, and 2 m/s and is tested on speeds that are 2 m/s or more

higher than the training speed range. (iii) change in the delay spread: if DeepRx is trained on low delay spreads such as 10, 50, and 80 ns and tested on higher delay spreads such as 400 ns. The explored configurations that led to a *performance drop* for DeepRx are summarized in Table I.

Next, we introduce VERITAS that automatically detects performance drop cases during the deployment of AI-native receiver, without having the true bit labels.

IV. VERITAS FOR VERIFYING THE PERFORMANCE OF AI-NATIVE RECEIVERS

In this section, we describe VERITAS as a framework for verifying the performance of AI-native receiver in the AI-AI. We first discuss the overview of the system and provide high level description of interactions between different components in Section IV-A. Next, we go into the details of *the Monitor*, and *the Performance Comparator* in Sections IV-B and IV-C, respectively.

A. System Overview

AI-native receivers interpret received signals into bit sequences. As shown in Fig. 1 VERITAS that is placed in parallel to the AI-native receiver, consists of 3 different components of *the Monitor*, *the Performance Comparator*, and the TradRx (introduced in Section III-A). The Monitor is pretrained on the same training set as the AI-native receiver. Therefore, the specific channel profile, speed, and delay spread covered in the training set are considered ID data for the Monitor NN. The Monitor constantly runs in parallel to the AI-native receiver (i.e., DeepRx) and detects any changes in the wireless channel as OOD samples. Following this detection one could retrain the AI-native receiver to adapt it to the new environment and restore its performance, however, not all the environment changes might cause a performance drop in the AI-native receiver, and retraining might be unnecessary. To avoid unnecessary retraining, as soon as the Monitor detects an environment change, the Performance Comparator is activated and triggers TradRx to run as the reference point for a certain period of time, in parallel to the AI-native receiver. The Performance Comparator compares bit probabilities generated by TradRx and the AI-native receiver, and decides if the AI-native receiver is still outperforming TradRx. Obviously, this performance comparison happens based on only bit probabilities, without having the true bit labels. If the AI-native receiver is outperforming TradRx, no retraining is required, and the Monitor should continue observing the wireless channel to detect future potential changes. If the AI-native receiver is not outperforming TradRx, a retraining process is initiated to adapt the AI-native receiver to the new environment. If a retraining process is initiated for the AI-native receiver, the Monitor needs to be retrained as well to update its set of ID classes and be able to continue detecting further changes in the wireless channel.

B. Environment Change Detector: Monitor

The job of the Monitor is to observe the wireless channel and detect potential changes in the channel profile, speed,

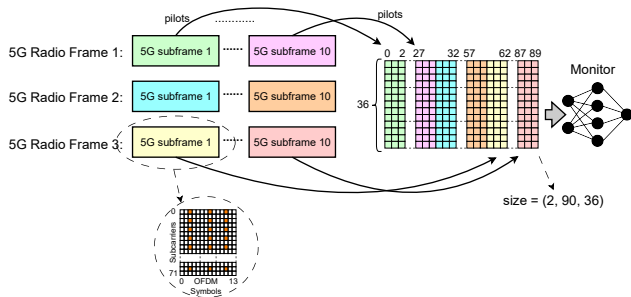


Fig. 10: To construct each input for the Monitor NN, received pilots in three 5G radio frames are concatenated to form input tensors with size $(2, 90, 36)$.

or delay spread. Based on this task, we design the Monitor to be a feature extractor NN attached to an OOD detection algorithm. Among the different methods that exist for OOD detection [21], [20], we select a feature-based OOD detection method from the post-hoc category, due to implementation simplicity and efficiency. In this method, an NN is designed and trained with triplet loss function to learn the in-distribution (ID) data classes, without getting exposed to any representation of OOD data during training. During deployment, test input features from one of the hidden layers are extracted, and are compared against the features of ID data in the training set, to make ID versus OOD decision for each input. This comparison can be done through different metrics. Inspired by [29], we propose an OOD detection algorithm based on the K-nearest neighbor (KNN) [30], and we use euclidean distance as our metric. The proposed method shows high performance in detecting far OOD data, as well as near OOD. In the following, we describe the input and outputs of the Monitor NN in Section IV-B1, describe the Monitor NN architecture and training and test processes in Section IV-B2, and describe the proposed OOD detection algorithm for detecting environment changes in Section IV-B3.

1) *Input and Output Structure*: Here, we assume the Monitor NN as a black box and explain how inputs for such NN are prepared.

Input. The environment change detection happens by processing only the frequency domain representation of the received 5G pilots. Specifically, we create a 3D matrix of 5G received pilots using pilots of 3 consecutive frames. Preparing the input to the Monitor component does not impose additional signal processing steps to the system, as the received frequency domain pilots are already prepared as an input component to DeepRx. Depending on the selected pilot pattern (see Fig. 2), the number of pilot columns will be different which leads to different input sizes for the Monitor NN. In our selected pilot pattern (explained in Section III-A) each OFDMA subframe consists of complex-valued pilots with dimension 36 along the frequency axis and dimension 3 along the time axis. We take pilot matrices from all the 10 subframes in 3 consecutive 5G radio frames and concatenate them along the time axis. We separate the real and imaginary parts of the pilots, and to be compliant with “channel first” configuration in PyTorch, we bring this dimension of 2 to the beginning. Consequently, we

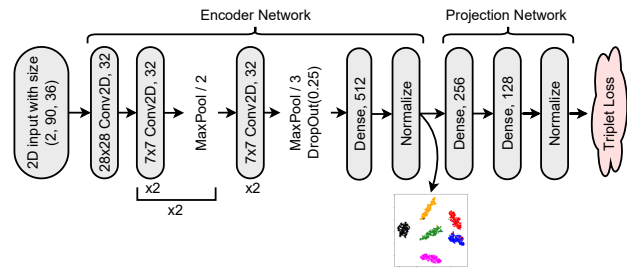


Fig. 11: The Monitor NN architecture with $\sim 600k$ parameters that consists of an encoder network and a projection network. Both networks are cascaded during training with triplet loss function. During deployment, the clusters are derived from the output of the encoder network.

form a matrix (tensor) of size $(2, 90, 36)$ that is the input to the Monitor NN. The process of preparing inputs for the Monitor NN using 3 consecutive 5G radio frames each comprising 10 subframes (with pattern (c) in Fig. 2) is shown in Fig. 10.

Output. Output of the Monitor is a binary decision (ID or OOD) per input tensor.

2) *Architecture and Training Process*: For the Monitor NN architecture, we cascade a custom designed encoder network that is in charge of feature extraction and a projection network that contributes to more processing to form more distinguishable and less scattered features.

Our encoder network is a convolutional NN with residual blocks, consisting of convolutional, maxpooling, dense (or fully connected), and dropout layers. We design the output layer of encoder network to be of size $I=512$, and normalize its output tensor using the normalization function $f_{\text{norm}}(x)$ in (1) before sending it out as y .

$$f_{\text{norm}}(x) = \frac{x}{\max(|x|)} \quad (1)$$

We note that the output of the encoder network, y , is a vector of I elements, however, we do not denote its vector indexing in this paper for the sake of simplicity.

Our projection network consists of two dense (i.e., fully connected) layers, and similar to the encoder network, we normalize its output tensor using (1) before sending it out of the projection network.

For training the Monitor, both encoder and projection networks are involved and cascaded together. We train the Monitor architecture with triplet loss function which is a supervised contrastive loss that requires three features of anchor, positive, and negative as inputs. The anchor and positive features are generated using two different input samples in the same class, and the negative feature is generated using a sample input from a different class. The triplet loss function tries to map the anchor and positive input samples into the same cluster, and the negative input sample into a distinct cluster. After training, we discard the projection network and only use the encoder network to generate features, ys . The Monitor NN architecture with two parts of encoder network and projection network is shown in Fig. 11.

We train 3 different Monitor NNs to detect changes in 3 different parameters of channel profile, transmitter speed, and delay spread. Our Monitor NN and training and test processes are implemented in Python using PyTorch libraries.

3) *OOD Detection Algorithm*: To distinguish a change in the wireless channel or environment, that is equivalent to identifying 5G pilot matrices as ID or OOD, we propose a non-parametric algorithm based on KNN, that processes the output features of the encoder network, y_s . As the network is trained with triplet loss function, our algorithm assumes that features generated from inputs of the same ID classes fall in the same cluster, and features generated from inputs of different ID classes form distinct clusters. In the following, we describe the processes of characterizing ID clusters and fitting a KNN algorithm that happen pre-deployment and ID/OOD decision making for each test sample that happens at the deployment phase.

Characterizing ID Clusters: The multidimensional ID clusters are created by passing the ID classes (i.e., the training set) through the fully trained encoder network, in the pre-deployment phase. In a training dataset with J ID classes indexed with $j = 0, \dots, J - 1$, where each ID class has population N_j , output features of the encoder network are denoted as $y_j^{(n)}$ with $n = 0, \dots, N_j - 1$. Each ID cluster needs to be characterized with a center, c_j , that is a vector of size I and a radius, r_j , that is a scalar. In this case, we gather all output vectors, $y_j^{(n)}$ s belonging to each ID class j , and calculate a center, c_j , for each ID cluster using (2).

$$c_j = \frac{1}{N_j} \sum_{n=0}^{N_j-1} y_j^{(n)}, \quad j = 0, 1, \dots, J - 1 \quad (2)$$

This equation simply calculates an I -dimensional mean for all the I -dimensional features in each ID class. To calculate cluster radius, r_j , associated with each ID class indexed with j in the training set, we calculate the euclidean distance of all training features, $y_j^{(n)}$ s, from c_j , and sort them in a list in the ascending order. We discard the last $1 - \lambda$ portion of the list and keep the first λ portion. The portion that is discarded is associated with features that are far away from the cluster center, c_j . We pick the last (i.e., largest) value of the remaining list as the cluster radius, r_j . We set λ to a large value such as 95%, so that the distance of 95% of the ID features to the cluster center, c_j , is smaller than the cluster radius, r_j (i.e., 95% of ID features fall inside their respective cluster). The aforementioned steps for characterizing each cluster by a center and a radius are summarized in Algorithm 1.

Fitting the KNN Algorithm. As the final step in the pre-deployment phase, we combine all the ID features from different ID classes in a set and fit a KNN algorithm to them, using the Python API `NearestNeighbors()`.

Making ID/OOD Decision for Each Test Sample: At the deployment phase, the Monitor is tested on input samples that might belong to an ID class or might be OOD. For each output vector y_{test} generated using each test input, we find its K nearest neighbors, each denoted as neighbor_k with $k = 0, \dots, K - 1$. Obviously, each of these neighbors belong to one of the ID classes. For each neighbor_k belonging to the

Algorithm 1: Characterizing In Distribution (ID) Clusters

- 1: **Inputs**: Trained encoder network, Training set containing all ID classes
 - 2: Set λ as 95%
 - 3: Pass the training set through the trained encoder network and collect the ID features $y_j^{(n)}$ s
 - 4: `center_list`, `radius_list` = [], []
 - 5: **for all** class j in ID classes **do**
 - 6: Calculate cluster center c_j using (2)
 - 7: `center_list.append(cj)`
 - 8: **for all** $y_j^{(n)}$ s indexed with n belonging to class j **do**
 - 9: `distance_list` = []
 - 10: Calculate euclidean distance of $y_j^{(n)}$ from its own cluster center c_j
 - 11: Append it as a scalar to `distance_list`
 - 12: **end for**
 - 13: Sort the `distance_list` in the ascending order
 - 14: Discard the last $1 - \lambda$ and pick the last element as r_j
 - 15: `radius_list.append(rj)`
 - 16: **end for**
 - 17: **Outputs**: `center_list`, `radius_list`
-

Algorithm 2: Out of Distribution (OOD) Detection

- 1: **Inputs**: `center_list`, `radius_list`, test feature y_{test}
 - 2: Return K nearest neighbors as `neighbor_list` = $\bigcup_{k=0}^{K-1} \text{neighbor}_k$
 - 3: **for** neighbor_k in `neighbor_list` **do**
 - 4: Calculate d_k as euclidean distance of neighbor_k from its own cluster center c_j
 - 5: Calculate d_y as euclidean distance of y_{test} from neighbor_k 's cluster center c_j
 - 6: **if** ($d_y \leq d_k$ **and** $d_y \leq r_j$) **then**
 - 7: $v_k = \text{ID}$
 - 8: **else**
 - 9: $v_k = \text{OOD}$
 - 10: **end if**
 - 11: `vote_list.append(vk)`
 - 12: **end for**
 - 13: **if** ID in `vote_list` **then**
 - 14: $v_{\text{final}} = \text{ID}$
 - 15: **else**
 - 16: $v_{\text{final}} = \text{OOD}$
 - 17: **end if**
 - 18: **Output**: v_{final}
-

ID class j , we find the euclidean distance of neighbor_k to its corresponding cluster center c_j , and denote it as d_k . We also calculate the euclidean distance of y_{test} from neighbor_k 's associated cluster center, c_j , and denote it as d_y . After this, we take a vote from each neighbor_k belonging to ID class j , determining whether the test output feature y_{test} belongs to class j or not. We check 2 criteria to get the vote of neighbor_k

denoted as v_k , as in (3):

$$v_k = \begin{cases} \text{ID} & \text{if } d_y \leq d_k \text{ and } d_y \leq r_j \\ \text{OOD} & \text{otherwise} \end{cases} \quad (3)$$

As shown in (3), a feature, y_{test} , is voted as ID by neighbor $_k$ if the euclidean distance of that feature to the cluster center of the neighbor is smaller or equal to the distance of the neighbor to its cluster center, and the distance of the feature from the cluster center of the neighbor is smaller than the cluster radius. Otherwise, the sample is voted as OOD by that neighbor.

We derive a final joint vote, v_{final} , for each y_{test} using the votes from its K neighbors as in (4).

$$v_{\text{final}} = \begin{cases} \text{ID} & \text{if any } v_k = \text{ID}, \quad k = 0, \dots, K - 1 \\ \text{OOD} & \text{otherwise} \end{cases} \quad (4)$$

Basically, we identify each sample as OOD if none of its nearest neighbors vote it to be ID with respect to their own ID clusters. The steps to identify each test sample as ID or OOD is summarized in Algorithm 2.

The highlights of the proposed OOD algorithm with respect to the state-of-the-art proposed in [29] and [25] are as follows:

- Our proposed OOD detection algorithm (Section IV-B3) performs well in sparse clusters with lower density in the center and higher density around the edges, due to being dependent on the ID cluster center and radius instead of the distance of the test sample from its nearest ID neighbors.
- Our proposed algorithm utilizes triplet loss (Section IV-B2) instead of supervised contrastive loss [31] used in [29] during training that allows for good OOD detection rate as well as low false positive rate among the samples detected as OOD.
- We use a custom NN architecture for OOD detection and show that the non-parametric feature-based OOD detection is applicable to 5G wireless data besides the benchmark image datasets of CIFAR, SVHN, etc. used in [29].

If the Monitor detects a change in the environment, the Performance Comparator is activated that is described next.

C. Performance Comparator

The job of the Performance Comparator in VERITAS is to decide whether or not DeepRx needs to be retrained. It compares the bit probabilities generated by TradRx and DeepRx to determine which receiver is generating lower BER, and initiates a retraining process only if DeepRx gives lower BER. Obviously, this comparison happens using predicted bit probabilities without involving true bit labels. The Performance Comparator is able to operate on probabilities associated with encoded as well as unencoded bits, which obviates the need to include a costly decoding operation in VERITAS.

As soon as the Performance Comparator is activated by the Monitor, it triggers the TradRx and runs it in parallel to DeepRx to decode the same received 5G radio frames for a specific time duration. We collect the softbits (LLRs) out of both receivers in this time duration, and convert them

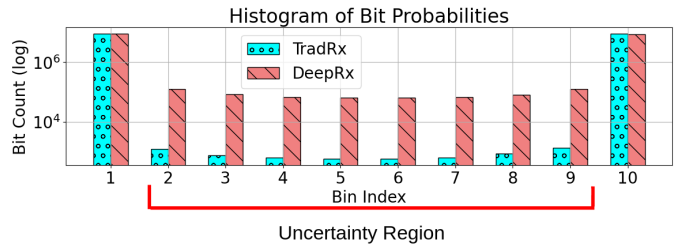


Fig. 12: Histogram of 4.5 million bit probabilities generated by passing the same test set through TradRx and DeepRx.

to bit probabilities. Bit probability P is calculated using its corresponding LLR through (5).

$$P = \frac{1}{1 + e^{\text{LLR}}} \quad (5)$$

In the hard decoding method, if P is less than or equal to 0.5 the bit is translated to logical '0', and if P is greater than 0.5 the bit is translated to logical '1'. Since the same received 5G radio frames are passed through DeepRx and TradRx, ideally the same bit probabilities should be generated by both receivers. However, we discover that in practice this is not the case. We find bit probabilities of TradRx and DeepRx to be different for the same test set, and even more, we find these probabilities to be related to each receiver's BER. We derive an empirical method based on our findings that is inspired by histogram binning approach [32], which is a basic scheme for calibrating NN predicted probabilities. In our approach we only use the "binning" concept without performing any sort of calibration or modification to the NN bit probabilities. We describe the proposed method in the following.

We note that each bit probability is a value between 0 and 1. We break the range of 0 to 1 to 10 chunks, creating 10 bins indexed with b that are associated with non-overlapping ranges, as in (6).

$$\text{bin}_b : \begin{cases} [\frac{b-1}{10}, \frac{b}{10}) & b = 1, 2, 3, \dots, 9 \\ [\frac{b-1}{10}, \frac{b}{10}] & b = 10 \end{cases} \quad (6)$$

Next, we categorize all the output bits from TradRx and DeepRx into these bins, based on their probability values, and count the number of bits in each bin. The histogram created for 4.5 million bits is shown in Fig. 12. In such a histogram, bin_1 and bin_{10} represent the most certain predictions for logical bits '0' and '1', respectively. On the other hand, bin_2 to bin_9 represent less certain predictions. We refer to these lower probability bins as the *uncertainty region*. We sum the bit counts in the uncertainty region and refer to them as U_{DeepRx} and U_{TradRx} for DeepRx and TradRx, respectively. The histogram bars in Fig. 12 are plotted for an example 5G radio frame dataset with transmitter speed set as 20 m/s and E_b/N_0 as 20 dB (the same dataset studied in Fig. 7 in Section III-C2). For this dataset, DeepRx provides larger BER compared to TradRx, and accordingly, in Fig. 12 DeepRx shows higher bit count in the uncertainty region compared to TradRx ($U_{\text{DeepRx}} = 680\text{k}$ versus $U_{\text{TradRx}} = 6\text{k}$). Statistical analysis over the whole test set of 500 5G radio frames (4.5 million bits) in different test speeds and different E_b/N_0 levels, verifies the

Algorithm 3: Performance Comparator for DeepRx and TradRx

- 1: **Inputs:** LLR_{DeepRx} , LLR_{TradRx}
 - 2: Convert LLR_{DeepRx} and LLR_{TradRx} to P_{DeepRx} and P_{TradRx} , respectively, using (5)
 - 3: Create histogram bins for both P s using (6)
 - 4: Calculate U_{DeepRx} as sum of the bit count in bin_2 to bin_9 , for DeepRx outputs
 - 5: Calculate U_{TradRx} as sum of the bit count in uncertainty region (bin_2 to bin_9), for TradRx outputs
 - 6: **if** $U_{DeepRx} \leq U_{TradRx}$ **then**
 - 7: Retraining = not needed
 - 8: **else**
 - 9: Retraining = needed
 - 10: **end if**
 - 11: **Output:** Retraining
-

same relation between bit probabilities and bit errors: *the receiver with the larger U (i.e., taller histogram bars) has worse performance (i.e., higher BER)*. However, to comply with this observation, we require to run TradRx and DeepRx in parallel for 500 5G radio frames and collect 4.5 million bits, only to determine the underperforming receiver and potentially trigger retraining. This imposes significant elapsed time to VERITAS and might cause many cyclic redundancy check (CRC) fails before determining the underperforming receiver, which in turn reduces the overall communication throughput. The important question is *What is the smallest bit population that is consistent with our observations regarding the relation of bit probabilities and receiver BER?* We evaluate the Performance Comparator and answer this question in Section V-B.

The algorithm describing the Performance Comparator that takes LLRs of both receivers and returns a decision about whether or not the retraining of DeepRx is required, is shown in Algorithm 3.

V. EVALUATIONS

In this section, we evaluate the performance of different components in VERITAS for change in 3 different parameters of channel profile, transmitter speed, and delay spread. We evaluate the Monitor and the Performance Comparator in Section V-A and Section V-B, respectively.

A. Environment Change Detector: Monitor

We train the Monitor NN for different problems of detecting change in the channel profile, in the transmitter speed, and in the delay spread. After each training, to visualize the extracted 512-dimensional features, we use a dimension reduction algorithms called t-SNE [33] to reduce feature dimensions to 2, and plot them as scatter plots. We should note that, t-SNE is used only for visualization, and Algorithms 1 and 2 are run on the 512-dimensional features, without any dimension reduction. We describe the details and results of experiments for detecting a change in the channel profile, transmitter speed, and delay spread in Sections V-A1, V-A2, and V-A3, respectively.

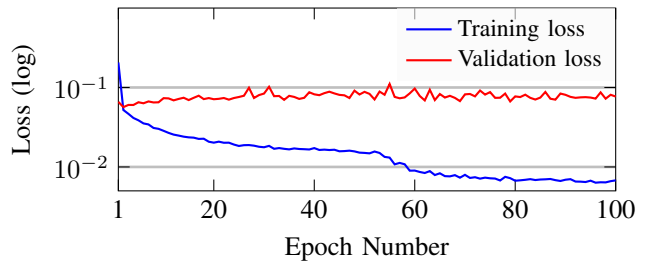


Fig. 13: Monitor NN training and validation losses over 100 epochs when it is trained on tdl_d and Uniform Noise, to detect change in the channel profile.

1) *Detecting a Change in the Channel Profile:* We evaluate our Monitor NN with data configured by getting guided by DeepRx performance described in Section III-C3, shown in Fig. 5 and summarized in Table I. As we observe, DeepRx *performance drop* happens if DeepRx is trained on tdl_d (LOS) and tested on tdl_a, tdl_b, and tdl_c. Therefore, one desired change detection is the transition between tdl_d channel profile to either one of the profiles tdl_a, tdl_b, or tdl_c. Based on this, we train the Monitor NN shown in Fig. 11 on the training dataset with configurations discussed in Section III-C1 that has only tdl_d channel profile. For training with triplet loss, the training set requires to contain more than one class, to be able to feed to the loss function similar (positive) and contrasting (negative) inputs with respect to the anchor. This second class cannot be based on any of the unseen classes, but should ideally have a different distribution from the first class. Therefore, we artificially synthesize a second class using the tdl_d training samples and use it as auxiliary data to train the Monitor NN. To form the second class, we take the pilot matrix for each 5G radio frame for tdl_d class, and calculate the minimum and maximum value of pilots among the combination of real and imaginary parts, as u_{min} and u_{max} , respectively. Then we create a new matrix with the same dimension of the tdl_d pilot matrix, and fill it with Uniform Noise in range $\sim U(u_{min}, u_{max})$. We train the Monitor NN to form distinct clusters for tdl_d pilot matrices and this auxiliary data that is derived from tdl_d with Uniform Noise distribution. We train the Monitor NN for 100 epochs with triplet loss on these two classes (a.k.a., as tdl_d and Uniform Noise) and show training and validation losses in Fig. 13.

After training, we detach the encoder network and use it in the test phase. Ideally the fully trained encoder network should be able to form distinct vectors (clusters) of dimension $I = 512$ for different ID classes and OOD data. To illustrate this, we test the trained encoder on our test ID and OOD data, extract features at the output of the encoder network, and perform t-SNE to reduce the dimensions of the features from $I = 512$ to 2D and enable visualization. In Fig. 14, we plot the 2D clusters for all test ID and OOD channel classes, for 3 different Eb/N0 levels of 0, 10, and 20 dB. We observe that the ID classes of tdl_d (LOS) and Uniform Noise form distinct clusters. Regarding the OOD classes, we see that features for all NLOS profiles of tdl_a, tdl_b, and tdl_c fall in the same space but form completely distinct clusters from the ID classes.

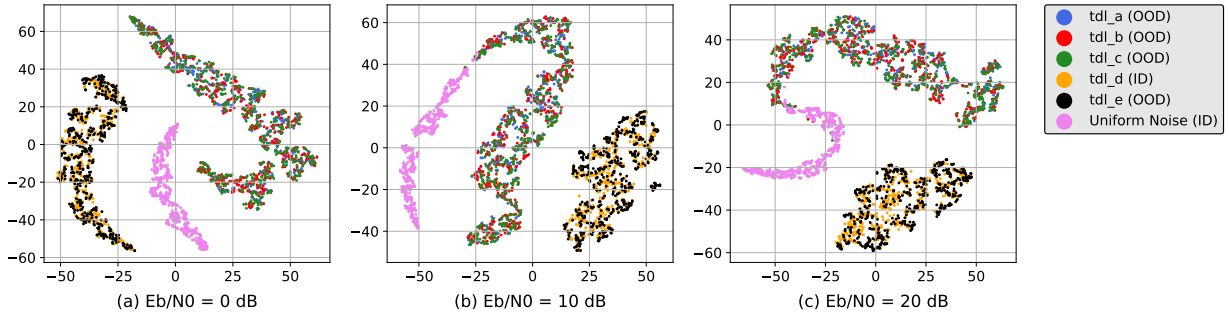


Fig. 14: t-SNE representation of feature vectors at the output of the encoder network as part of the Monitor for detecting the change in channel profiles. The clusters are shown for different ID and OOD channel profile classes at 3 different E_b/N_0 levels of (a) 0, (b) 10, and (c) 20 dB.

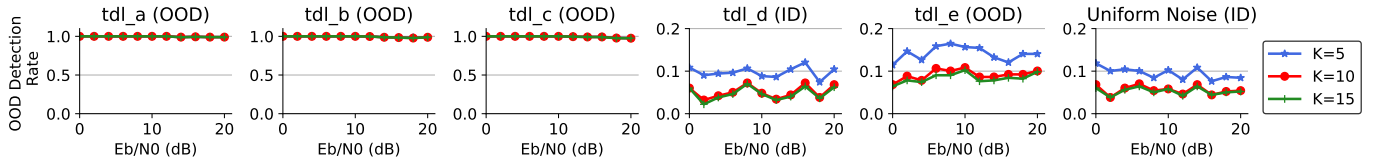


Fig. 15: OOD detection rate for different test channel profiles with three different nearest neighbor parameters of $K = 5, 10, 15$. We observe high detection rate for OOD channels and low rate for ID channels. In the case of tdl_e that is an OOD channel, we observe low OOD detection rate, which is consistent with overlapping tdl_d and tdl_e clusters in Fig. 14.

We can see that tdl_e (LOS) cluster completely overlaps with the ID cluster tdl_d (LOS). The reason for this is that tdl_e channel profile is very similar to the ID class tdl_d . We can also see the impact of this similarity in Fig. 5, where DeepRx model is trained on tdl_d (LOS), but still performs better than TradRx when it is tested on the unseen tdl_e (LOS) channel profile. This also shows that not being able to distinguish the ID class tdl_d from the OOD class tdl_e is not a problem, since DeepRx is indifferent to the transition from tdl_d to tdl_e , and maintains its high performance with respect to TradRx. Furthermore, the distinct ID and OOD clusters in all low, medium, and high E_b/N_0 levels in Fig. 14(a), (b), and (c), respectively, can be justified by two reasons: First, the pattern of input to the Monitor that is the psuedo random sequence of 5G pilots with QPSK modulation scheme is a simple pattern and it is not much affected by noise up to $E_b/N_0=0$ dB. Second, the Monitor is trained on all E_b/N_0 levels in the range of 0 to 20 dB with steps of 2 dB, and hence good cluster distinction is observed in all E_b/N_0 levels.

To numerically evaluate how separable the ID and OOD clusters are, we pass the training set that contains ID classes through the trained encoder network in the Monitor NN and record the ID features. We characterize each of the 512 dimensional ID clusters by a 512 dimensional center c_j , and a scalar radius r_j through Algorithm 1. We run the OOD detection algorithm described in Algorithm 2 with 3 different K nearest neighbor values of 5, 10, and 15, on the unseen test set that is a combination of all ID and OOD classes. We calculate OOD detection rate for each test class and each K at each E_b/N_0 level. In Fig. 15, we observe that the OOD classes of tdl_a , tdl_b , and tdl_c whose clusters are separate from ID classes achieve 97%+ OOD detection rate in all E_b/N_0 levels for all K values. The average OOD detection

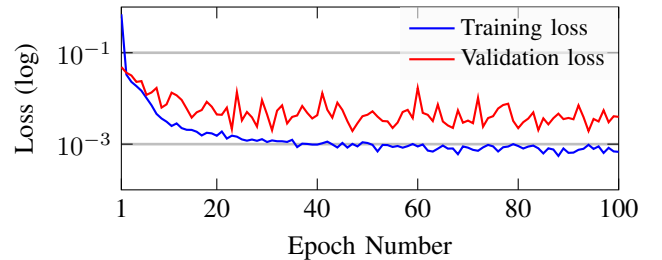


Fig. 16: Monitor NN training and validation losses over 100 epochs when it is trained on the speeds of 0, 1 and 2 m/s, to detect change in the transmitter speed.

rate for these NLOS channels over all E_b/N_0 levels is 99%+ for all K values. We also observe that the ID classes of tdl_d and Uniform Noise achieve a low OOD detection rate, which means low rate of false positives. This low rate reduces from 9.7% to 4.7% as we increase K from 5 to 15. As expected from the overlapping clusters of tdl_d (ID) and tdl_e (OOD) in Fig. 14, tdl_e does not achieve a high OOD detection rate. However, mistaking the OOD class tdl_e for the ID class tdl_d does not create a problem for DeepRx as explained before and summarized in Table I.

2) *Detecting a Change in Transmitter Speed:* Similar to Section V-A1, to define our ID and OOD speed classes, we are guided by DeepRx performance for the change in transmitter speed that is studied in Section III-C2 in Fig. 7, and summarized in Table I. We train the Monitor NN for 100 epochs on speeds 0, 1, and 2 m/s and show the training and validation losses in Fig. 16.

Similar to Section V-A1, to illustrate clusters, we test the trained encoder network on the unseen test set that contains

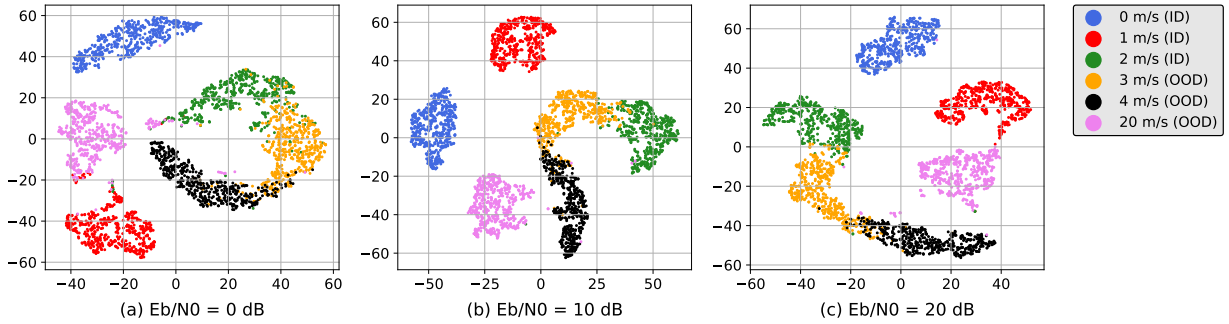


Fig. 17: t-SNE representation of feature vectors at the output of the encoder network as part of the Monitor for detecting the change in transmitter speed. The clusters are shown for different ID and OOD speed classes at 3 different E_b/N_0 levels of (a) 0, (b) 10, and (c) 20 dB.

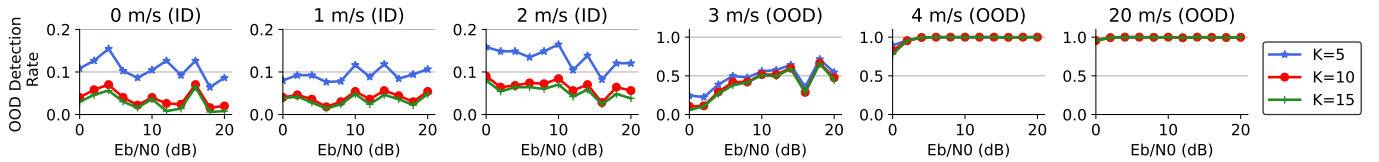


Fig. 18: OOD detection rate for different test transmitter speeds with three different nearest neighbor parameters of $K = 5, 10, 15$. We observe low detection rate for ID speeds of 0, 1, and 2 m/s and high rate for OOD speeds of 4 and 20 m/s. In the case of 3 m/s that is an OOD speed, we observe low OOD detection rate, which is consistent with close and touching clusters of 2 and 3 m/s in Fig. 14.

ID speeds of 0, 1, and 2 m/s, and OOD speeds of 3, 4, and 20 m/s. We extract features out of the encoder network, reduce the feature dimensions using t-SNE transform, and plot the ID and OOD 2D clusters for three E_b/N_0 levels of 0, 10 and 20 dB in Fig. 17. We can see that different ID classes of 0, 1, 2 m/s form independent and distinct clusters. Also the OOD class of 3 m/s that is the closest to the ID class of 2 m/s (a.k.a., near OOD) forms a cluster right next to that of 2 m/s. Similarly, the other OOD class of 4 m/s that is close to 3 m/s forms another cluster next to that of 3 m/s. However, the 20 m/s OOD data that is a speed far from any of the ID speeds (a.k.a., far OOD) forms a completely independent cluster with respect to those of the ID or other OOD classes. Again, the clusters maintain their distinction from each other in lower E_b/N_0 levels too, as explained in Section V-A1.

For numerical evaluation, similar to Section V-A1, we collect ID features for speeds 0, 1, and 2 m/s using the training set, and characterize each of the 512 dimensional clusters by a 512 dimensional center c_j , and a scalar radius r_j , using Algorithm 1. We pass the test set that is a combination of unseen samples from ID and OOD classes through the trained encoder network and run the Algorithm 2 to detect OOD features. We measure OOD detection rate for different ID classes of 0, 1, and 2 m/s and different OOD classes of 3, 4, and 20 m/s and plot them in Fig. 18, for different nearest neighbor parameter K set as 5, 10, and 15. We observe that for ID classes we achieve low OOD detection rate across different E_b/N_0 levels which is desirable as it shows low false positive rate. We see that increasing K from 5 to 15 reduces the average OOD detection rate from 10% to 2%, from 9% to 3%, and from 13% to 5% for ID classes of 0, 1, and 2 m/s,

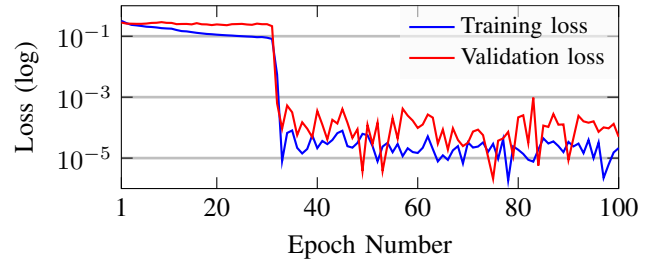


Fig. 19: Monitor NN training and validation losses over 100 epochs when it is trained on delay spreads of 10, 50 and 80 ns, to detect change in the delay spread.

respectively. For OOD speeds of 4 and 20 m/s we observe high OOD detection of 97%+ averaged over all E_b/N_0 levels, for different K values. However, for the near OOD speed of 3 m/s, the OOD detection rate does not achieve higher than 47% with varying the K value. This phenomenon is expected as the 3 m/s OOD cluster in Fig. 17 is located right next to the 2 m/s ID cluster, and without distinct colors these two clusters might not be visually separable. Therefore, it is expected that OOD samples of 3 m/s are sometimes mistaken for the ID sample of 2 m/s, which decreases the OOD detection rate for 3 m/s. However, this does not create a problem in VERITAS as the DeepRx model trained on a specific training speed range can still maintain its superior performance over TradRx, if it is tested on speeds 1 m/s higher than the training range (see Table I).

3) *Detecting a Change in Delay Spread*: Similar to Sections V-A1 and V-A2 to form our ID and OOD classes for the delay spread parameter, we are guided by DeepRx

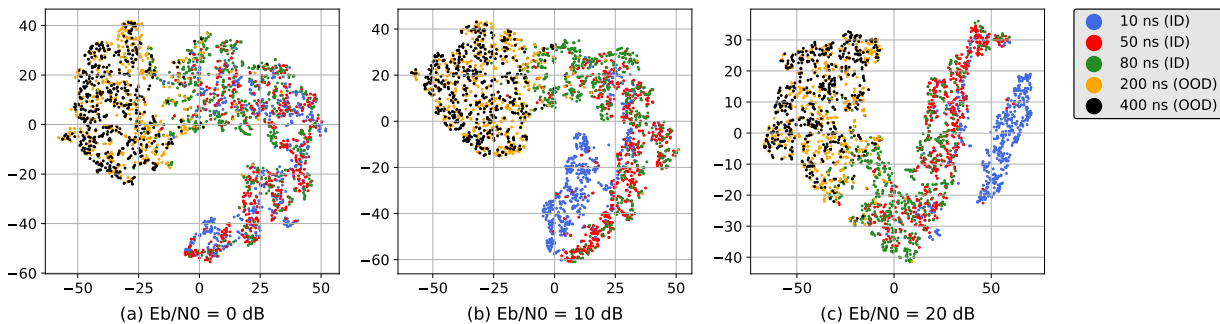


Fig. 20: t-SNE representation of feature vectors at the output of the encoder network as part of the Monitor for detecting the change in delay spread. The clusters are shown for different ID and OOD delay spread classes at 3 different E_b/N_0 levels of (a) 0, (b) 10, and (c) 20 dB.

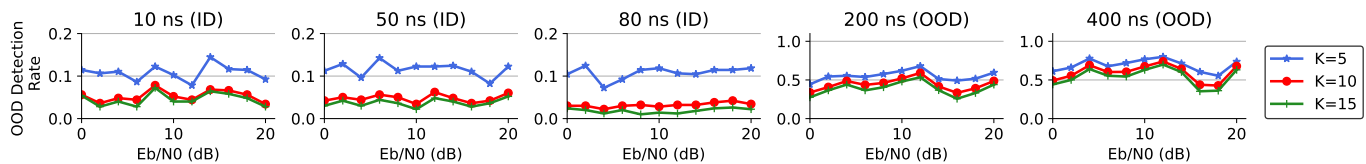


Fig. 21: OOD detection rate for different test delay spreads with three different nearest neighbor parameters of $K = 5, 10, 15$. We observe low OOD detection rates (false positives) for ID delay spreads of 10, 50, and 80 ns and higher rates for OOD delay spreads of 200 and 400 ns, which is consistent with clusters shown in Fig. 20.

performance for change in the delay spread that is studied in Section III-C3 in Fig. 9 and summarized in Table I. We train the Monitor NN for 100 epochs on the training set with delay spreads 10, 50 and 80 ns and show the training and validation losses in Fig. 19.

Similar to Sections V-A1 and V-A2 to illustrate clusters, we test the trained encoder network on the delay spread test set consisting of ID delay spreads of 10, 50, and 80 ns and OOD delay spreads of 200 and 400 ns. We extract test set features out of the encoder network, reduce the 512 dimension to 2 dimensions using t-SNE, and plot the clusters for three E_b/N_0 levels of 0, 10, and 20 dB in Fig. 20. We observe that with increasing the E_b/N_0 level, some of the clusters, specially the ID cluster of 10 ns, occupy a more independent space. However, all the clusters of ID and OOD are closer to each other compared to Fig. 14 and Fig. 17 and are more difficult to distinguish even in high E_b/N_0 levels. Because of this, we expect to see lower OOD detection rate for OOD classes.

To measure OOD detection rate for all classes, we test the trained encoder network with the training set and form the 512 dimensional clusters for ID classes. For each cluster, we calculate a 512-dimensional cluster center c_j and a scalar radius r_j using Algorithm 1. We test the trained encoder on the unseen test set that is a combination of ID and OOD classes, calculate OOD detection rate versus different E_b/N_0 levels for different ID and OOD classes and different nearest neighbor parameter of $K = 5, 10, 15$, and plot them in Fig. 21. We observe low OOD detection rate for ID classes of 10, 50, and 80 ns, which shows low false positive rate. We also observe that increasing K from 5 to 15 reduces the average OOD detection rate from 10% to 4%, from 11% to 3%, and from 10% to 1% for ID classes of 0, 1, and 2 m/s, respectively. For

OOD classes of 200 and 400 ns, the highest OOD detection rate we observe is 55% and 69%, respectively, with $K = 5$. This relatively lower OOD detection rate is consistent by the more intertwined clusters in Fig. 20, compared to the distinct clusters in Fig. 14 and Fig. 17.

One key take away from Fig. 15, Fig. 18, and Fig. 21 is that increasing K from 5 to 15 has a more significant impact on decreasing the OOD detection rate for the ID classes (a.k.a., false positive rate) compared to increasing OOD detection rate for OOD classes (a.k.a., true positive rate). This is consistent with the nature of the proposed OOD detection algorithm described in IV-B3, where each test sample is identified as “ID” even if only one neighbor identifies it as ID, and therefore, increasing the number of neighbors, K , has a large impact on each test sample being identified as ID.

B. Performance Comparator

To evaluate the Performance Comparator that determines whether retraining DeepRx is required or not, we extract LLRs and calculate bit probabilities of DeepRx and TradRx, for all the test experiments of Channel Profile - Exp. 2, Speed - Exp. 2, and Delay Spread - Exp. 2 in Section III-C. As it can be seen in Fig. 15, Fig. 18, and Fig. 21, for channel profile, transmitter speed, and delay spread, respectively, any of the inputs with ID or OOD true labels might be predicted as OOD, even if it is with a low probability in the case of inputs with ID true labels. This means that the proposed Performance Comparator needs to correctly determine if DeepRx requires retraining for all ID and OOD classes. To evaluate this, we define an accuracy metric for the Performance Comparator, based on the output from Algorithm 3. We evaluate the Performance Comparator on a per-frame basis, which means we collect the LLRs from

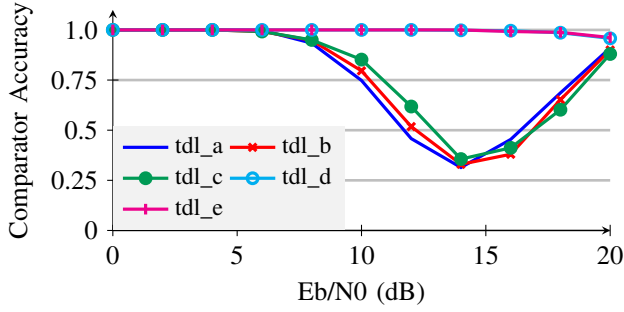


Fig. 22: Comparator accuracy when DeepRx is trained on tdl_d, and 5G frames with different channel profiles are passed through the trained DeepRx and TradRx.

DeepRx and TradRx for one 5G radio frame with 6 PBRs per subframe that is equivalent to 36k softbits from each receiver, and feed them to Algorithm 3. The 36k that is the number of softbits in each 5G radio frame is achieved through the following calculations:

$$10 [\text{subframes}] \times 4 [16\text{QAM modulation}] \times (72 \times 14 - 36 \times 3) [\text{data without pilots}] = 36000$$

The Performance Comparator component determines whether or not DeepRx needs retraining once for every 5G radio frame (i.e., one prediction per 5G radio frame). In Algorithm 3, we consider each prediction as a correct decision if the Performance Comparator flags retraining as “needed” and in fact $\text{BER}_{\text{DeepRx}} > \text{BER}_{\text{TradRx}}$ for the corresponding frame, or if it flags retraining as “not needed” and in fact $\text{BER}_{\text{DeepRx}} \leq \text{BER}_{\text{TradRx}}$ for that corresponding frame. We calculate Performance Comparator accuracy for each test set as the number of correct decisions divided by the total number of decisions. We show Performance Comparator accuracy for different ID and OOD test sets of different channel profiles, transmitter speeds, and delay spreads in Sections V-B1, V-B2, and V-B3.

1) *Performance Comparator Accuracy in Different Channel Profiles:* In Fig. 22, where DeepRx is trained on tdl_d channel profile, we observe Performance Comparator accuracies of 77%, 77%, 78%, 99%, and 99%, averaged over all Eb/N0 levels, for test channel profiles of tdl_a, tdl_b, tdl_c, tdl_d, and tdl_e, respectively. This can be averaged to 86% accuracy for all the test channel profiles in all Eb/N0 levels. Lowest accuracy of 31-35% can be seen for the NLOS channel profiles of tdl_a, tdl_b, and tdl_c, in Eb/N0=14 dB. Comparing this with Fig. 5 shows the low accuracy happens close to the Eb/N0 level that the two BER graphs of DeepRx and TradRx cross (i.e., 12 dB). This means the Performance Comparator makes incorrect decisions regarding whether or not retraining is required mostly when $\text{BER}_{\text{DeepRx}} \approx \text{BER}_{\text{TradRx}}$. At Eb/N0=14 dB where we have the lowest Performance Comparator accuracy for tdl_a, tdl_b, and tdl_c, $\text{BER}_{\text{DeepRx}}$ is only 2.6×10^{-3} higher than $\text{BER}_{\text{TradRx}}$. Therefore, an incorrect decision of “retraining not required” hurts the system BER by only 2.6×10^{-3} higher BER, for ~70% of the frames.

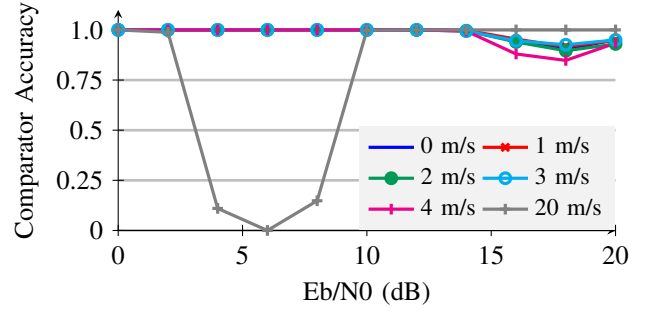


Fig. 23: Comparator accuracy when DeepRx is trained on 0, 1, and 2 m/s speeds, and 5G frames with different speeds are passed through the trained DeepRx and TradRx.

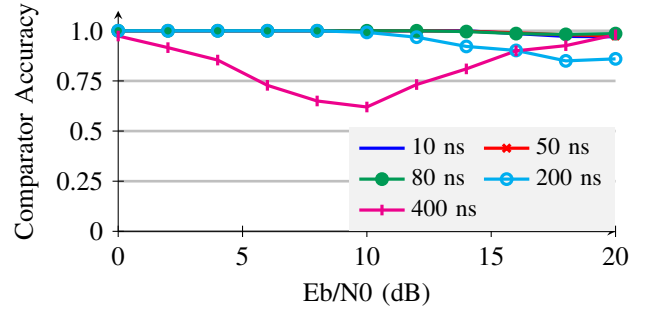


Fig. 24: Comparator accuracy when DeepRx is trained on 10, 50, and 80 ns delay spreads, and 5G radio frames with different delay spreads are passed through the trained DeepRx and TradRx.

2) *Performance Comparator Accuracy in Different Transmitter Speeds:* In Fig. 23, where DeepRx is trained on speeds 0, 1, and 2 m/s, we observe comparator accuracies of 98%, 98%, 97%, 98%, 96%, and 75%, averaged over all Eb/N0 levels, for test speeds of 0, 1, 2, 3, 4, and 20 m/s, respectively. This can be averaged to 93.3% accuracy for all the test speeds in all Eb/N0 levels. Lowest accuracy of 0% can be seen for the highest speed of 20 m/s in Eb/N0=6 dB. Comparing this with Fig. 7 shows the low accuracy happens close to the Eb/N0 level that the two BER graphs of DeepRx and TradRx cross (i.e., 4 dB). This means the comparator makes incorrect decisions regarding whether or not retraining is required mostly when $\text{BER}_{\text{DeepRx}} \approx \text{BER}_{\text{TradRx}}$. At Eb/N0=6 dB, where we have the lowest Performance Comparator accuracy for speed 20 m/s, $\text{BER}_{\text{DeepRx}}$ is only 1.4×10^{-2} higher than $\text{BER}_{\text{TradRx}}$. Therefore, an incorrect decision of “retraining not required” hurts the system BER by only 1.4×10^{-2} higher BER.

3) *Performance Comparator Accuracy in Different Delay Spreads:* In Fig. 24, where DeepRx is trained on delay spreads 10, 50, and 80 ns, we observe comparator accuracies of 99%, 99%, 99%, 95%, and 82%, averaged over all Eb/N0 levels, for test delay spreads of 10, 50, 80, 200, and 400 ns, respectively. This can be averaged to 94.8% accuracy for all the test delay spreads in all Eb/N0 levels. Lowest accuracy of 62% can be seen for the highest delay spread of 400 ns in Eb/N0=10 dB. Comparing this with Fig. 9 shows the low accuracy happens close to the Eb/N0 level where the two BER graphs

of DeepRx and TradRx cross (i.e., 6 dB). This means the comparator makes incorrect decisions regarding whether or not retraining is required mostly when $BER_{DeepRx} \approx BER_{TradRx}$. At $E_b/N_0=10$ dB where we have the lowest Performance Comparator accuracy for delay spread 400 ns, BER_{DeepRx} is only $1.0e-2$ higher than BER_{TradRx} . Therefore, an incorrect decision of “retraining not required” hurts the system BER by only $1.0e-2$ higher BER for only $\sim 38\%$ of the 5G radio frames.

VI. CONCLUSION

In this paper, we proposed VERITAS as a framework for verifying the performance of NN-based receivers in the AI-AI. VERITAS consists of a Monitor, a Performance Comparator, and a traditional receiver as the reference point. The Monitor that is an OOD detector NN constantly observes the wireless channel. The Monitor detects changes in different parameters of the channel including the channel profile (i.e., LOS or NLOS environment), transmitter speed, and delay spread. The proposed Monitor shows 99%, 97%, and 69% OOD detection rate for channel profile, transmitter speed, and delay spread, respectively. As soon as a change in the wireless channel is detected, the Monitor activates a TradRx to be used as a reference receiver that runs in parallel to the NN-based receiver. The Performance Comparator compares the bit probabilities yielding from the same data inputs passing through DeepRx and TradRx and identifies the underperforming receiver in terms of BER, to determine whether or not a retraining process needs to be started. The Performance Comparator correctly triggers retraining with an average accuracy of 86%, 93.3%, and 94.8% for all channel profile, transmitter speed, and delay spread test sets, averaged over all E_b/N_0 levels.

REFERENCES

- [1] J. Hoydis, F. A. Aoudia, A. Valcarce, and H. Viswanathan, “Toward a 6G AI-Native Air Interface,” *IEEE Communications Magazine*, vol. 59, no. 5, pp. 76–81, 2021.
- [2] Ericsson, “Defining AI native: A key enabler for advanced intelligent telecom networks.” <https://www.ericsson.com/en/reports-and-papers/white-papers/ai-native>.
- [3] N. Soltani, H. Cheng, M. Belgiovine, Y. Li, H. Li, B. Azari, S. D’Oro, T. Imbiriba, T. Melodia, P. Closas, *et al.*, “Neural Network-Based OFDM Receiver for Resource Constrained IoT Devices,” *IEEE Internet of Things Magazine*, vol. 5, no. 3, pp. 158–164, 2022.
- [4] B. Azari, H. Cheng, N. Soltani, H. Li, Y. Li, M. Belgiovine, T. Imbiriba, S. D’Oro, T. Melodia, Y. Wang, *et al.*, “Automated Deep Learning-Based Wide-Band Receiver,” *Computer Networks*, vol. 218, p. 109367, 2022.
- [5] A. Al-Shawabka, F. Restuccia, S. D’Oro, T. Jian, B. C. Rendon, N. Soltani, J. Dy, S. Ioannidis, K. Chowdhury, and T. Melodia, “Exposing the Fingerprint: Dissecting the Impact of the Wireless Channel on Radio Fingerprinting,” in *IEEE INFOCOM 2020-IEEE Conference on Computer Communications*, pp. 646–655, IEEE, 2020.
- [6] N. Soltani, K. Sankhe, J. Dy, S. Ioannidis, and K. Chowdhury, “More Is Better: Data Augmentation for Channel-Resilient RF Fingerprinting,” *IEEE Communications Magazine*, vol. 58, no. 10, pp. 66–72, 2020.
- [7] F. Meng, P. Chen, L. Wu, and X. Wang, “Automatic Modulation Classification: A Deep Learning Enabled Approach,” *IEEE Transactions on Vehicular Technology*, vol. 67, no. 11, pp. 10760–10772, 2018.
- [8] P. Jiang, T. Wang, B. Han, X. Gao, J. Zhang, C.-K. Wen, S. Jin, and G. Y. Li, “AI-aided OFDM Receiver: Design and Experimental Results,” *arXiv preprint arXiv:1812.06638*, 2018.
- [9] F. A. Aoudia and J. Hoydis, “End-to-end Learning for OFDM: From Neural Receivers to Pilotless Communication,” *IEEE Transactions on Wireless Communications*, 2021.
- [10] J. Zhang, C.-K. Wen, S. Jin, and G. Y. Li, “Artificial Intelligence-aided Receiver for a CP-free OFDM System: Design, Simulation, and Experimental Test,” *IEEE Access*, vol. 7, pp. 58901–58914, 2019.
- [11] Z. Zhao, M. C. Vuran, F. Guo, and S. Scott, “Deep-waveform: A Learned OFDM Receiver Based on Deep Complex Convolutional Networks,” *arXiv preprint arXiv:1810.07181*, 2018.
- [12] H. Ye, G. Y. Li, and B.-H. Juang, “Power of Deep Learning for Channel Estimation and Signal Detection in OFDM Systems,” *IEEE Wireless Communications Letters*, vol. 7, no. 1, pp. 114–117, 2017.
- [13] X. Gao, S. Jin, C.-K. Wen, and G. Y. Li, “ComNet: Combination of Deep Learning and Expert Knowledge in OFDM Receivers,” *IEEE Communications Letters*, vol. 22, no. 12, pp. 2627–2630, 2018.
- [14] B. Azari, H. Cheng, N. Soltani, H. Li, Y. Li, M. Belgiovine, T. Imbiriba, S. D’Oro, T. Melodia, Y. Wang, *et al.*, “Automated Deep Learning-based Wide-band Receiver,” *Computer Networks*, vol. 218, p. 109367, 2022.
- [15] M. Honkala, D. Korpi, and J. M. Huttunen, “Deeprx: Fully convolutional deep learning receiver,” *IEEE Transactions on Wireless Communications*, vol. 20, no. 6, pp. 3925–3940, 2021.
- [16] M. B. Fischer, S. Dörner, F. Krieg, S. Cammerer, and S. ten Brink, “Adaptive NN-based OFDM Receivers: Computational Complexity vs. Achievable Performance,” in *2022 56th Asilomar Conference on Signals, Systems, and Computers*, pp. 194–199, IEEE, 2022.
- [17] M. Belgiovine, K. Sankhe, C. Bocanegra, D. Roy, and K. Chowdhury, “Deep Learning at the Edge for Channel Estimation in Beyond-5G Massive MIMO,” *IEEE Wireless Communications Magazine*, pp. 1–7, 2021.
- [18] M. Elwekeil, T. Wang, and S. Zhang, “Deep Learning for Environment Identification in Vehicular Networks,” *IEEE Wireless Communications Letters*, vol. 9, no. 5, pp. 576–580, 2019.
- [19] I. Saffar, M. L. A. Morel, K. D. Singh, and C. Vihoo, “Deep Learning Based Speed Profiling for Mobile Users in 5G Cellular Networks,” in *2019 IEEE Global Communications Conference (GLOBECOM)*, pp. 1–7, IEEE, 2019.
- [20] J. Zhang, J. Yang, P. Wang, H. Wang, Y. Lin, H. Zhang, Y. Sun, X. Du, K. Zhou, W. Zhang, *et al.*, “OpenOOD v1.5: Enhanced Benchmark for Out-of-Distribution Detection,” *arXiv preprint arXiv:2306.09301*, 2023.
- [21] J. Yang, K. Zhou, Y. Li, and Z. Liu, “Generalized Out-of-Distribution Detection: A Survey,” *arXiv preprint arXiv:2110.11334*, 2021.
- [22] J. Liu, T. Oyedare, and J.-M. Park, “Detecting Out-of-Distribution Data in Wireless Communications Applications of Deep Learning,” *IEEE Transactions on Wireless Communications*, vol. 21, no. 4, pp. 2476–2487, 2021.
- [23] J. Robinson and S. Kuzdeba, “Novel Device Detection using RF Fingerprints,” in *2021 IEEE 11th Annual Computing and Communication Workshop and Conference (CCWC)*, pp. 0648–0654, IEEE, 2021.
- [24] DARPA, “Radio Frequency Machine Learning Systems.” <https://www.darpa.mil/program/radio-frequency-machine-learning-systems>.
- [25] G. Shen, J. Zhang, A. Marshall, and J. R. Cavallaro, “Towards Scalable and Channel-Robust Radio Frequency Fingerprint Identification for LoRa,” *IEEE Transactions on Information Forensics and Security*, vol. 17, pp. 774–787, 2022.
- [26] Google, “TensorFlow Lite.” <https://www.tensorflow.org/lite>.
- [27] GNU radio, “The Signal Metadata Format (SigMF).” <https://sigmf.org>.
- [28] National Instruments, “Prototyping a Real-Time Neural Receiver with USRP and OpenAirInterface.” <https://www.ni.com/en/solutions/electronics/5g-6g-wireless-research-prototyping/prototyping-real-time-neural-receiver-usrp-openairint.html>.
- [29] Y. Sun, Y. Ming, X. Zhu, and Y. Li, “Out-of-Distribution Detection with Deep Nearest Neighbors,” in *International Conference on Machine Learning*, pp. 20827–20840, PMLR, 2022.
- [30] L. E. Peterson, “K-Nearest Neighbor,” *Scholarpedia*, vol. 4, no. 2, p. 1883, 2009.
- [31] P. Khosla, P. Teterwak, C. Wang, A. Sarna, Y. Tian, P. Isola, A. Maschinot, C. Liu, and D. Krishnan, “Supervised Contrastive Learning,” *Advances in neural information processing systems*, vol. 33, pp. 18661–18673, 2020.
- [32] C. Guo, G. Pleiss, Y. Sun, and K. Q. Weinberger, “On Calibration of Modern Neural Networks,” in *International conference on machine learning*, pp. 1321–1330, PMLR, 2017.
- [33] L. Van der Maaten and G. Hinton, “Visualizing Data using t-SNE,” *Journal of machine learning research*, vol. 9, no. 11, 2008.